IET Renewable Power Generation

Special Issue Call for Papers

Be Seen. Be Cited.
Submit your work to a new IET special issue

Connect with researchers and experts in your field and share knowledge.

Be part of the latest research trends, faster.

Read more

The Institution of Engineering and Technology

Check for updates

Received: 9 January 2022 | Revised: 22 March 2022 | Accepted: 12 April 2022

IET Renewable Power Generation

DOI: 10.1049/rpg2.12487

The Institution of Engineering and Technology WILEY

ORIGINAL RESEARCH

Design and optimization of yokeless magnetic gear with asymmetric Halbach permanent magnet array for electric vehicle powertrain

Yuanxi Chen[1] | Xing Zhao[2] | Siulau Ho[1] | Shuangxia Niu[1] | Weinong Fu[3]

[1]Department of Electrical Engineering, The Hong Kong Polytechnic University, Hung Hom, Hong Kong

[2]Department of Electronic Engineering, University of York, York, UK

[3]Shenzhen Institutes of Advanced Technology, Chinese Academy of Sciences, Shenzhen, China

Correspondence:
Shuangxia Niu, Department of Electrical Engineering, The Hong Kong Polytechnic University, Hung Hom, Hong Kong. Hong Kong, 999077, China.
Email: eesxniu@polyu.edu.hk

Funding information
Research Grant Council of the Hong Kong SAR Government, Grant/Award Numbers: PolyU152180/19E, PolyU152185/18E

Abstract

In this paper, a novel 3/27/24 (pole pairs of inner rotor permanent magnet [PM]s/modulator/outer rotor PMs) high torque density yokeless magnetic gear with asymmetric Halbach PM array is presented and optimized for electric vehicle powertrain. The key is to improve the torque performance by replacing the magnetic steel with the light nonmagnetic material as the rotor core and employing the embedded magnetic steel bar as well as trapezoidal PM structure to form a low magnetic resistance in the magnetic circuit. The proposed machine has significant performance improvements in two aspects. Firstly, it has high torque density and low iron loss with the yokeless structure. Secondly, it has a high anti-saturation capability and low torque ripple with the asymmetric Halbach PM array and the embedded magnetic steel bar. The proposed structure is optimized by the co-simulation of the finite-element method and C++ optimization software. For a clear evaluation, the proposed structure is compared with generalized solutions in terms of performance and cost. Comparison results indicate that the proposed solution has the highest output torque, torque density, and torque per PM weight among solutions, reaching 214.1 N·m, 58.2 N·m/kg, and 95.6 N·m/kg, which greatly enhances the performance of the magnetic gear.

1 | INTRODUCTION

Magnetic gear (MG) provides the solution for replacing the mechanical gearbox in the electric vehicle propulsion system [1–5] for its inherent advantages of high transmission efficiency, overload protection, low working noise, and physical isolation [6–7]. To tap the potentials of industrial application, researchers focus on the MG, including radial-flux [8–10] MG, axial-flux MG [11, 12], and magnetic-geared machines [13–15], for finding the better performance solutions. However, due to the limit of machine structures, all those MGs employ rotor iron cores to form the magnetic circuit and reduce the magnetic reluctance, which becomes the major weight of the machine. For compensating inherent drawbacks, the yokeless structure has been proposed and applied in MG. However, the yokeless structure leads to poor performance of MG inevitably with the removal of iron cores since it increases the magnetic reluctance and introduces a great leakage flux. For solving this problem, the papers [16–19] proposed the types of MGs with the Halbach PM array, focusing on the arrangement and design of it. A yokeless MG with Halbach PM array for lessening the reliance on iron cores is shown in Figure 1c compared with the conventional MG and yokeless MG shown in Figures 1a and 1b, which can reduce the leakage flux to some degree. Compared with the conventional solution, the yokeless structures use glass fibre reinforced polymer (GFRP) with the density of 1.1 g/cm^3 and operating temperature of 115° to replace the magnetic steel (7.8 g/cm^3) as the material of rotor cores. However, the Halbach structure cannot solve the leakage flux issue altogether as the magnetic circuit still needs to contain the air gap, which will lead to a large magnetic reluctance. Hence, although the generalized design and research in this topology have made some progress, in terms of its design thought, the improvement level is very limited.

This is an open access article under the terms of the Creative Commons Attribution License, which permits use, distribution and reproduction in any medium, provided the original work is properly cited.
© 2022 The Authors. *IET Renewable Power Generation* published by John Wiley & Sons Ltd on behalf of The Institution of Engineering and Technology.

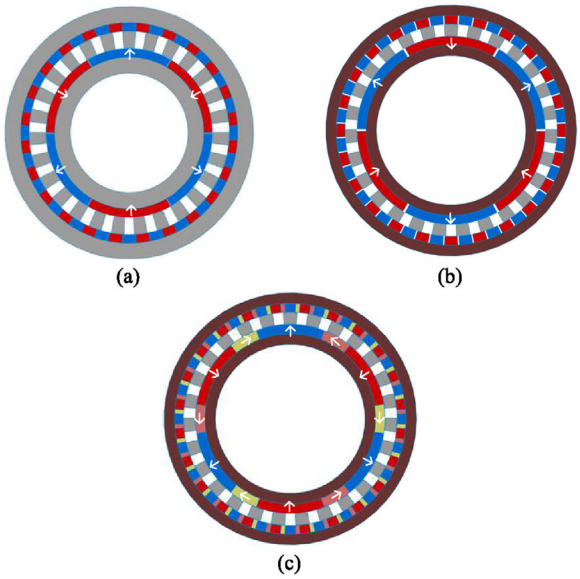

FIGURE 1 Structure comparison of MGs. (a) Conventional MG. (b) Yokeless MG. (c) Yokeless MG with Halbach PM array. MG, magnetic gear; PM, permanent magnet

In this paper, a novel yokeless MG with asymmetric Halbach PM array consisting of trapezoidal Halbach PM array and embedded magnetics steel bar is proposed to overcome the shortcomings mentioned above. The trapezoidal structure is employed to further reduce the output ripple and the embedded magnetic steel bar installed in the radially magnetized PM is to reduce the magnetic reluctance as well as to improve the torque performance. Besides, the thickness of the yokeless MG's rotor core can be reduced only if it has sufficient mechanical strength for maintaining the operation of MG, which further reduces the weight and improves the torque density.

2 | ANALYTICA MODELLING OF THE PROPOSED GEAR

In this section, the design of the asymmetric Halbach PM arrangement and the equivalent magnetic circuit is derived. The discussion in this section is divided into the following aspects:

1) The yokeless structure design, mechanical strength consideration, and the operating principle are analyzed carefully.

2) The general pattern of the Halbach PM arrangement is analyzed and conducted. The magnetization of the asymmetric Halbach PM array and the equivalent magnetic circuit are deduced.

2.1 | Structure configuration and operating principle analysis

The overall structure of the proposed yokeless MG with the asymmetric trapezoidal Halbach PM array is shown in Figure 2,

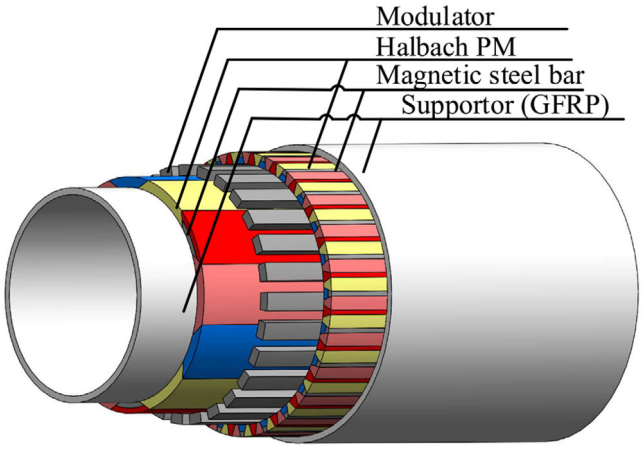

FIGURE 2 Topology of the proposed yokeless MG with asymmetric structure consisting of Halbach PM array and embedded magnetic steel bar

which contains four kinds of magnetized PMs, GFRP supporters, and embedded magnetic steel bar.

The thickness of the rotor core can be reduced to a certain level only if it has sufficient mechanical strength for maintaining the operation of MG. In this paper, GFRP is employed as the material of iron core (supporter), which has a tensile strength of 53.9–75.5 MPa (1 N/mm^2). The affordable torque of the supporter should follow (1):

$$\sigma b = \frac{T}{SL} \tag{1}$$

where σb, T, S, and L are the ultimate strength, torque, stressed area, and the length of force, respectively. Hence, the thickness of the rotor is selected as 2.5 mm, which can tolerate more than 2000 N·m acting on the rotor.

All MGs or magnetic-geared machine, including the proposed structure, should comply with the fundamental rule, which is expressed as (2)

$$P = N_{\mathrm{L}} + N_{\mathrm{H}} \tag{2}$$

where N_{L} and N_{H} are the numbers of pole pairs of the low-speed rotor (LSR) and high-speed rotor (HSR), P is the number of modulators.

For getting a higher torque, P should be equal to $N_{\mathrm{H}} + N_L$ [20]. Similarly, the speeds of corresponding HSR and LSR should follow:

$$\frac{\omega_{\mathrm{H}}}{\omega_{\mathrm{L}}} = -\frac{N_{\mathrm{L}}}{N_{\mathrm{H}}} = G_{\mathrm{r}} \tag{3}$$

where ω_{L} is the mechanical speed of LSR while ω_{H} is that of high speed. The proportion G_{r} of the two speeds is the gear ratio, which means the speed ratio of the MG equals the inverse ratio of the PM pole-pair numbers of two rotors.

The fixed parameters of the proposed structure are shown in Table 1 and the others will be optimized and discussed in the next section.

17521424, 2022, 11, Downloaded from https://ietresearch.onlinelibrary.wiley.com/doi/10.1049/rpg2.12487 by Hong Kong Polytechnic University, Wiley Online Library on [27/08/2023]. See the Terms and Conditions (https://onlinelibrary.wiley.com/terms-and-conditions) on Wiley Online Library for rules of use; OA articles are governed by the applicable Creative Commons License

TABLE 1 Fixed parameters of the proposed machine

QUANTITY	Value
Radial diameter	110 mm
Axial length	110 mm
Air gap	0.5 mm
Number of pole pairs of PM in LSR	3
Number of pole pairs of PM in HSR	24
Number of modulators	27
Speed of LSR	300 rpm
Speed of HSR	2400 rpm

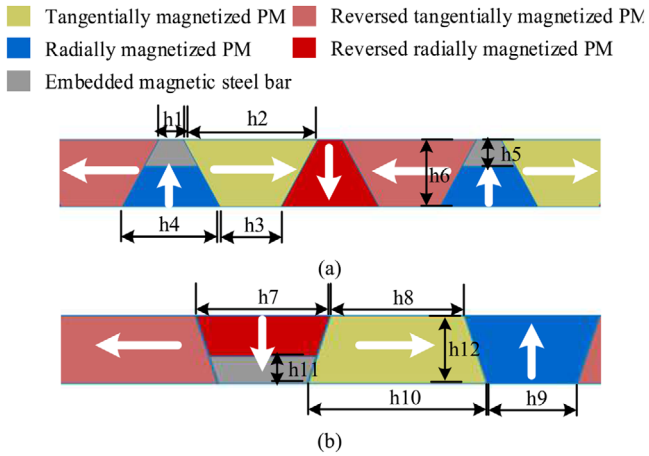

FIGURE 3 The asymmetric Halbach PM arrangement. (a) Outer rotor (low speed rotor). (b) Inner rotor (high speed rotor)

2.2 | The general pattern of asymmetric Halbach PM array

The proposed asymmetric Halbach PM array installed LSR and HSR is indicated in Figures 3a and 3b. The magnetized directions of PMs have four types, including radial, reversed radial, tangential, and reversed tangential indicated as the white arrows in the figure.

For the Halbach topology, the magnetization generated by radially and tangentially magnetized PMs can be expressed by Fourier series expansions as follows:

$$\vec{M}\ (\theta) = M_{\mathrm{T}}\ (\theta)\vec{i}_{\mathrm{T}} + M_{\mathrm{R}}\ (\theta)\vec{i}_{\mathrm{R}} \tag{4}$$

where M_{R} and M_{T} are the radial and tangential components of the magnetization while $\vec{i}_{\mathrm{T}}$ and $\vec{i}_{\mathrm{R}}$ are the unit vector in the radial and tangential directions.

However, the proposed asymmetric structure cannot be analyzed via (4) with the employment of the embedded magnetic steel bar and the trapezoidal structure. As for the former, the Fourier series-based magnetization model of the LSR internal field can be indicated as Figure 4.

The M_{LR}, M'_{LR}, and M_{LT} are the peak magnetization of radially magnetized PM with and without the embedded magnetic steel bar as well as the tangentially magnetized PM. The M_{LR} that is always larger than M'_{LR} for the magnetic steel bar will occupy space for installing, which reduces the volume of radially magnetized PMs in LSR inevitably.

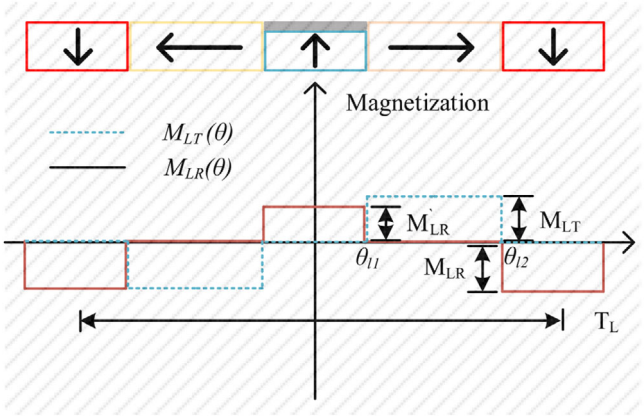

FIGURE 4 Fourier series expansion of trapezoidal Halbach magnetization model

$$\begin{cases} M_{LR}\ (\theta) = \dfrac{2}{\pi}\left(\displaystyle\int_0^{\theta_{l1}} M'_{LR}\cos(n\theta)\,d\theta - \int_{\theta_{l2}}^{T_{Lp}} M_{LR}\cos(n\theta)\,d\theta\right) \\ cos\left(np_L\theta\right) \\ M_{LT}\ (\theta) = \dfrac{2}{\pi}\displaystyle\int_{\theta_{l1}}^{\theta_{l2}} M_{LT}\cos(n\theta)\sin\left(np_L\theta\right) \end{cases} \tag{5}$$

The tangentially magnetized PM is perfectly symmetric, making the peak value of magnetization the same. The θ_1 and θ_2 are determined by the parameters h_n indicated in Figure 3. Hence, $M_{LT}(\theta)$ and $M_{LR}(\theta)$ can be rewritten as (5) where the p_L is the pole pairs of the PMs in the rotor. Similarly, the magnetization generated by the PMs in the HSR can be shown as

$$\begin{cases} M_{HR}\ (\theta) = \dfrac{2}{\pi}\left(\begin{array}{l} -\displaystyle\int_{\theta_{h2}}^{T_{Hp}} M'_{HR}\cos(n\theta)\,d\theta \\ +\displaystyle\int_0^{\theta_{h1}} M_{HR}\cos(n\theta)\,d\theta \end{array}\right)\cos\left(np_H\theta\right) \\ M_{LT}\ (\theta) = \dfrac{2}{\pi}\displaystyle\int_{\theta_{h1}}^{\theta_{h2}} M_{HT}\cos(n\theta)\sin\left(np_H\theta\right) \end{cases} \tag{6}$$

The trapezoidal structure has variable proportions varied to the distance from the central point of the machine. Hence, assuming that the h_5 is small enough, Equation (5) (6) needs to

17521424, 2022, 11, Downloaded from https://ietresearch.onlinelibrary.wiley.com/doi/10.1049/rpg2.12487 by Hong Kong Polytechnic University, Wiley Online Library on [27/08/2023]. See the Terms and Conditions (https://onlinelibrary.wiley.com/terms-and-conditions) on Wiley Online Library for rules of use; OA articles are governed by the applicable Creative Commons License

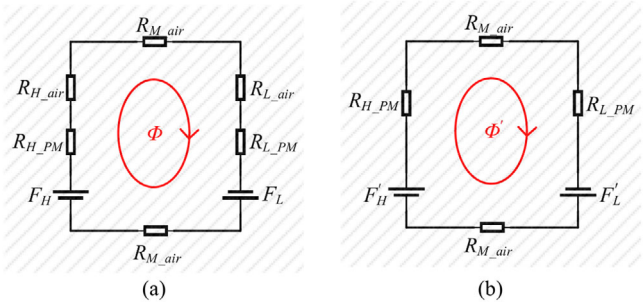

FIGURE 5 Equivalent magnetic circuit of the machine. (a) Without the embedded magnetic steel bar. (b) With the embedded magnetic steel bar

be revised as

$$\begin{cases} \vec{M}_{LR} = \int_{r-h_6}^{r} M_{LR}(\theta)\left(h_1 + \frac{r-l}{h_6}(h_4 - h_1)\right) dl \\ \vec{M}_{LT} = \int_{r-h_6}^{r} M_{LT}(\theta)\left(h_3 + \frac{r-l}{h_6}(h_2 - h_3)\right) dl \end{cases} \tag{7}$$

$$\begin{cases} \vec{M}_{HR} = \int_{r'-h_{12}}^{r'} M_{HR}(\theta)\left(h_9 + \frac{r-l}{h_{12}}(h_7 - h_9)\right) dl \\ \vec{M}_{HT} = \int_{r'-h_{12}}^{r} M_{HT}(\theta)\left(h_8 + \frac{r-l}{h_{12}}(h_{10} - h_8)\right) dl \end{cases} \tag{8}$$

where r is the radius of PMs and l is the distance between the bottom of PMs in LSR and the calculating points.

By regulating the parameters h_n, the useless harmonics of the magnetization $\vec{M}$could be reduced, which guarantees a low torque ripple of the proposed design, compared to conventional solutions with any pole pairs combination.

2.3 | Equivalent magnetic circuit analysis

The equivalent magnetic circuit of yokeless MG with and without the embedded magnetic steel bar is shown in Figure 5. The magnetomotive forces generated by the PMs installed in the two rotors and modulated by modulator are connected in series and the amplitudes of them have the same direction.

In Figure 5, the F_{H} and F_{L} are the magnetomotive forces generated by the HSR PM and LSR PM; $R_{\mathrm{H\_PM}}$, $R_{\mathrm{L\_PM}}$, and $R_{\mathrm{M_air}}$are the magnetic resistor of the HSR PM, LSR PM, and the air gap between rotors and modulators. Prominently, the MG has two same air gaps which provide two $R_{\mathrm{M\_air}}$ in the magnetic circuit. As for the yokeless MG without the embedded magnetic steel bar, there is a leakage flux outside of the LSR PM and inside of the HSR PM. It inevitable leads to a high magnetic resistance $R_{\mathrm{H\_air}}$ and $R_{\mathrm{L\_air}}$, which is shown in Figure 6.

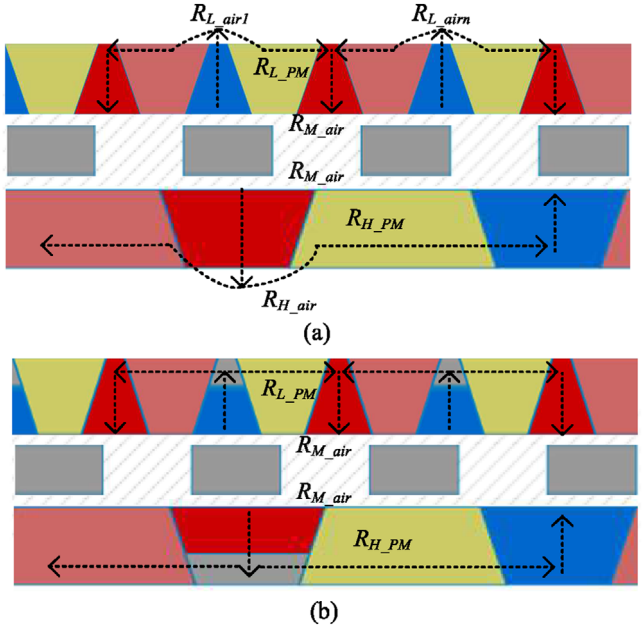

FIGURE 6 Magnetic resistor diagram of yokeless structure. (a) Without the embedded magnetic steel bar. (b) With the embedded magnetic steel bar

As shown in Figure 6, the proposed structure can reduce the magnetic resistors $R_{\mathrm{H\_air}}$ and $R_{\mathrm{L\_air}}$, which significantly improves the flux ϕ and performance of the yokeless MG. Although the magnetomotive force F will be reduced slightly with the installation of the magnetic steel bar, it can be solved by increasing the PMs volume slightly since the trapezoidal structure requires a very limited volume of magnetic steel bar.

This effectiveness of the proposed design can also be indicated as (9) and (10)

$$\phi = \frac{F_{\mathrm{H}} + F_{\mathrm{L}}}{2R_{\mathrm{M\_air}} + R_{\mathrm{H\_PM}} + R_{\mathrm{L\_PM}} + R_{\mathrm{H\_air}} + R_{\mathrm{H\_air}}} \tag{9}$$

$$\phi' = \frac{F'_{\mathrm{H}} + F'_{\mathrm{L}}}{2R_{\mathrm{M\_air}} + R'_{\mathrm{H\_PM}} + R'_{\mathrm{L\_PM}}} \tag{10}$$

As shown in (9) and (10), it can be easily indicated that the proposed structure has an inherent high flux with the same volume of PMs, which guarantees a high torque density of the proposed design compared to conventional solutions.

3 | OPTIMIZATION AND COMPARISON

In this section, the optimization algorithm is proposed and implemented via a co-simulation between the finite-element method and designed C++ software. The optimized parameters and calculation results are selected for finding the impacts of dimensional parameters on the proposed structure. The optimized targets are selected according to the torque density, the ripples of both rotors, as well as the PMs consumption.

17521424, 2022, 11, Downloaded from https://ietresearch.onlinelibrary.wiley.com/doi/10.1049/rpg2.12487 by Hong Kong Polytechnic University, Wiley Online Library on [27/08/2023]. See the Terms and Conditions (https://onlinelibrary.wiley.com/terms-and-conditions) on Wiley Online Library for rules of use; OA articles are governed by the applicable Creative Commons License

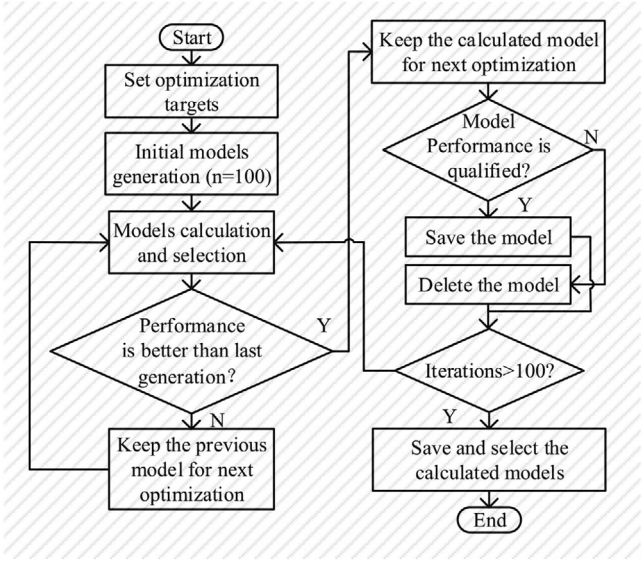

FIGURE 7 Designed optimization procedure of the proposed machine

3.1 | Optimization algorithm

The optimization procedure of the proposed machine is shown in Figure 7. The genetic algorithm (GA) is employed as the optimization algorithm [21–24].

Firstly, the optimization targets are set as the LSR torque, ripples of two rotors while the population quantity is selected as 100 considering the computing power.

Secondly, the models with different parameters are generated and calculated. After the calculation, the results are saved and selected based on the performance of optimized targets. If the performance of the calculated model is better than the previous generation, it will be kept for the next optimization or it will be deleted.

Thirdly, the qualification of the calculated model will be selected, preventing the computer from calculating unreasonable dimensional parameters and wasting computational resources.

Finally, if the iterations reach the set point, the optimization progress is finished. By introducing the co-simulation of optimization, a quantitative and detailed comparison between the conventional MG, yokeless MG, yokeless MG with Halbach PM array, and the proposed structure can be effectively conducted.

The range of the optimization parameters *h*1–h12 is shown in Table 2. Except the thickness of the PMs and the embedded magnetic steel bar (*h*5, *h*6, *h*11, and *h*12), the *hn* is defined as the proportion between the width of the normal Halbach PM array and the corresponding width of the trapezoidal structure.

3.2 | Optimized result comparison

The optimized parameters h_n are indicated in Figure 3. For getting a convenience optimized, the proportion of the relevant parameters is set and used in optimization.

TABLE 2 Optimization parameter ranges

Optimized quantity	Symbol	Range
LSR outer magnetic angle ratio	*h1/h2*	0.3–0.8
LSR inner magnetic angle ratio	*h4/h3*	1–1.7
LSR magnetic bar thickness ratio	*h5/h6*	0.2–0.4
HSR outer magnetic angle ratio	*h9/h10*	0.4–0.8
HSR inner magnetic angle ratio	*h7/h8*	0.7–1.7
HSR magnetic bar thickness ratio	*h11/h12*	0.2–0.4
LSR PMs thickness	*h6*	2.5–6 mm
HSR PMs thickness	*h12*	2.5–6 mm
HSR/LSR yoke thickness		3–8 mm
Modulator thickness		3–7 mm

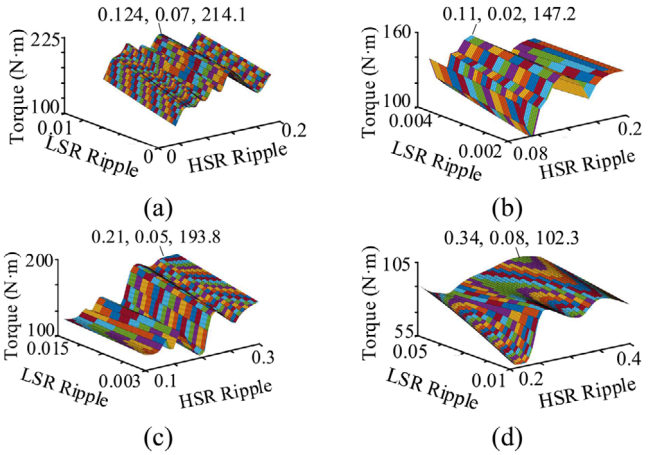

FIGURE 8 Optimization results of LSR torque versus LSR ripple and HSR ripple. (a) The proposed machine. (b) The conventional MG. (c) The yokeless MG with Halbach PM array. (d) The yokeless MG. HSR, high-speed rotor; LSR, low-speed rotor

As for the comparison models, the conventional MG, yokeless MG, yokeless MG with Halbach also be optimized via co-simulation. The optimization parameters include the thickness of PMs in two rotors, modulator, yoke the proportion between the modulator and its gap.

The optimization results of LSR torque versus LSR ripple and HSR ripple are shown in Figure 8. The proposed structure can achieve the largest output torque capacity and lowest ripple of both LSR and HSR under a fixed radial diameter and axial length shown in Table 1, reaching 214.1 N·m, 0.103, and 0.009 while the torque of the conventional MG, yokeless MG and yokeless MG with Halbach PM array only reach 174, 118, and 193.8 N·m. However, only the torque performance cannot verify the effectiveness of the proposed design, hence, LSR torque versus torque density and torque density with PM weight is also conducted, as shown in Figure 9.

As shown in Figure 9, the torque density and torque density with PMs of the proposed structure also has the best performance, reaching 58.20 and 95.65 N·m/kg and showing different advantages compared with those three comparison models.

17521424, 2022, 11, Downloaded from https://ietresearch.onlinelibrary.wiley.com/doi/10.1049/rpg2.12487 by Hong Kong Polytechnic University, Wiley Online Library on [27/08/2023]. See the Terms and Conditions (https://onlinelibrary.wiley.com/terms-and-conditions) on Wiley Online Library for rules of use; OA articles are governed by the applicable Creative Commons License

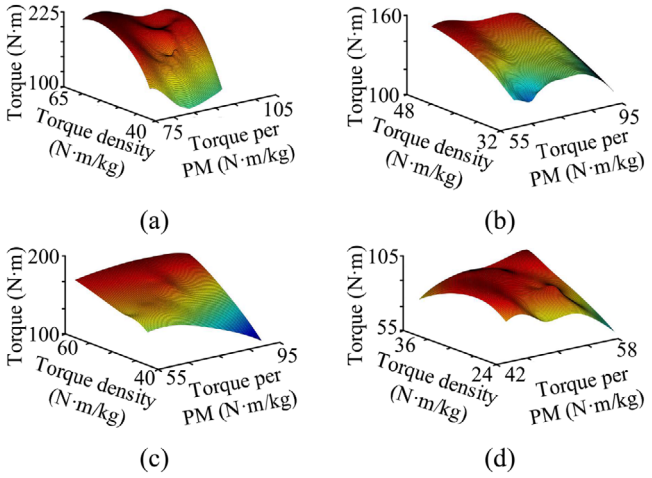

FIGURE 9 Optimization results of LSR torque versus torque density and torque density with PM weight. (a) The proposed machine. (b) The conventional MG. (c) The yokeless MG with Halbach PM array. (d) The yokeless MG

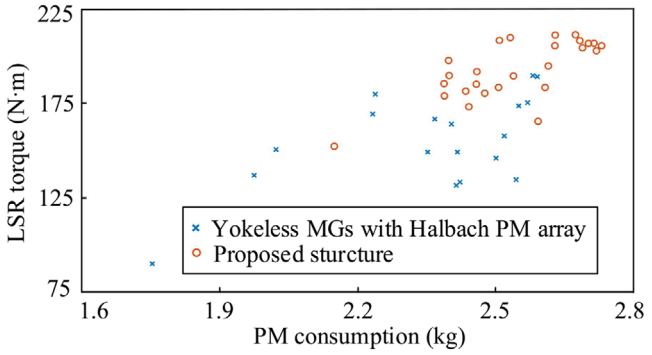

FIGURE 10 Optimization results of LSR torque versus PM consumption

Compared with the conventional MG with 46.1 N·m/kg of torque density, the proposed structure is with a significant improvement of 26.1% while the torque density with PM weight shows no significant difference.

As for the yokeless MG with Halbach PMs array, the proposed structure has a comprehensive advantage in both two aspects: improve the torque density and torque density with PMs' weight with 8.3% and 5.2%. The improvement seems not obvious; however, the optimization results indicate that the proposed structure has a better anti-saturation capacity: the output torque can increase linearly with the increase of PMs volume in a larger range while that of the yokeless MG with Halbach will stop increasing with a smaller volume of PMs, as indicated in Figure 10.

As shown in Figure 10, under a fixed volume of machine, the yokeless MG with Halbach PM array will be saturated when the PM consumption reaches about 2.24 kg, which means that the LSR torque cannot increase with the PM beyond that. Prominently, the LSR torque of the proposed structure can keep increasing if the PM is not more than 2.39 kg, extending the saturation point with an improvement of 6.7%.

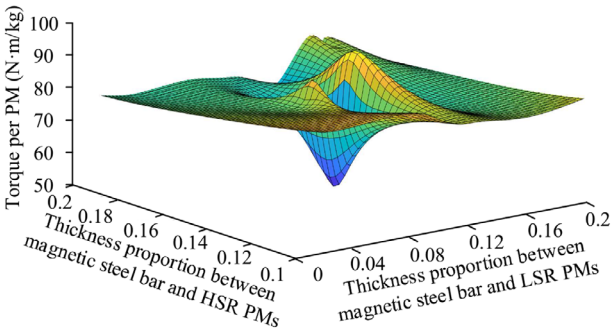

FIGURE 11 Optimization results of torque density with PMs weight versus thickness proportion between magnetic steel bar and PMs of LSR and HSR

TABLE 3 Optimized parameters of the proposed gear

Symbol	Quantity	Value
h6	Outer rotor PM thickness (mm)	4.8
h5	Outer rotor steel bar thickness (mm)	1.1
h12	Inner rotor PM thickness (mm)	6.6
h11	Outer rotor steel bar thickness (mm)	1.3
h1/h2	LSR outer magnetic angle ratio	0.75
h4/h3	LSR inner magnetic angle ratio	1.55
h9/h10	HSR outer magnetic angle ratio	0.75
H7/h8	HSR inner magnetic angle ratio	1.05
	Modulator thickness (mm)	3.5
	LSR magnetic bar thickness ratio	0.15
	LSR magnetic bar thickness ratio	0.15

Furthermore, compared with the yokeless MG, the proposed structure has overwhelming superiority in all torque, torque density, and torque density with PMs' weight, increasing more than 108.4%, 66.1%, and 66.3%, respectively. It also indicates a strong anti-saturation capacity of the proposed structure compared to yokeless MG.

The thickness proportion between the magnetic steel bar and the PMs of LSR and HSR will greatly impact the performance, which is the key optimization parameter in this progress. Figure 11 indicates the relation between the torque density with PMs and the proportion mentioned above.

The torque density with PMs peaks at the magnetic steel bar and PM proportion of LSR and HSR with 0.15 and 0.15, reaching 95.65 N·m/kg. Hence, after comparison and selection, the optimized dimensional combination is chosen and shown in Table 3 and the model with optimized parameters will be used in the next section for the performance analysis and compared with the other conventional solutions.

4 | PERFORMANCE ANALYSIS

In this section, the performance of the proposed structure will be analyzed and compared to the conventional MG, yokeless

17521424, 2022, 11, Downloaded from https://ietresearch.onlinelibrary.wiley.com/doi/10.1049/rpg2.12487 by Hong Kong Polytechnic University, Wiley Online Library on [27/08/2023]. See the Terms and Conditions (https://onlinelibrary.wiley.com/terms-and-conditions) on Wiley Online Library for rules of use; OA articles are governed by the applicable Creative Commons License

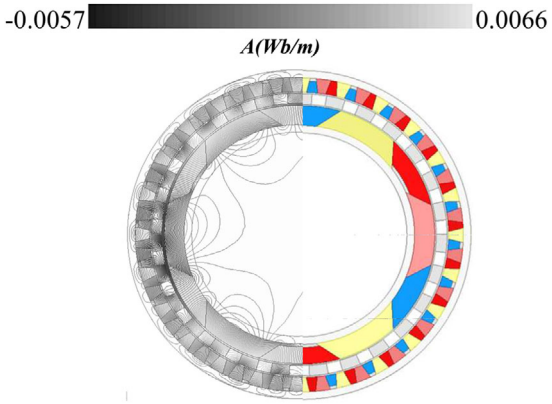

FIGURE 12 Magnetic flux lines distribution

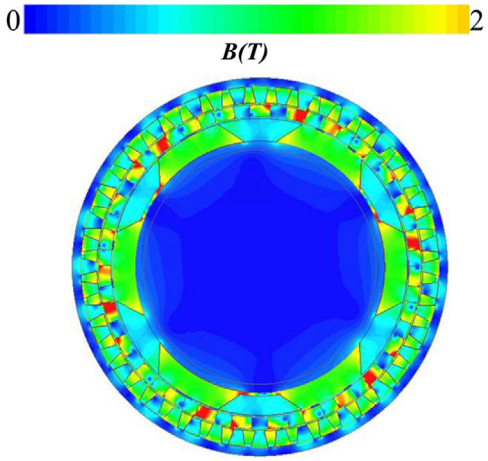

FIGURE 13 Flux density distribution under full load condition

MG, and yokeless MG with Halbach PM array, including the torque, loss, and efficiency.

4.1 | Magnetic field analysis

Figure 12 demonstrates the magnetic field distribution of the proposed structure calculated by FEA, whose linkage flux in both the outer side of LSR PM and the inner side of HSR PM is reduced significantly. Although the yokeless structure cannot fully reduce the linkage flux, however, with the introduction of the magnetic steel bar, more flux will be through it instead of through the air to form the magnetic circuit compared to the conventional solution shown in Figure 1.

Figure 13 shows the magnetic flux density of the proposed structure under the full load condition, verifying the effectiveness of the proposed design with a relatively low saturation status.

Figure 14 shows the harmonic spectra of inner and outer air gap flux density as well as the fast fourier transform (FFT) analysis results. The magnetic flux density in the inner air gap consists of both the third and 24th harmonics while the third dominates the flux density waveform, which meets the analysis

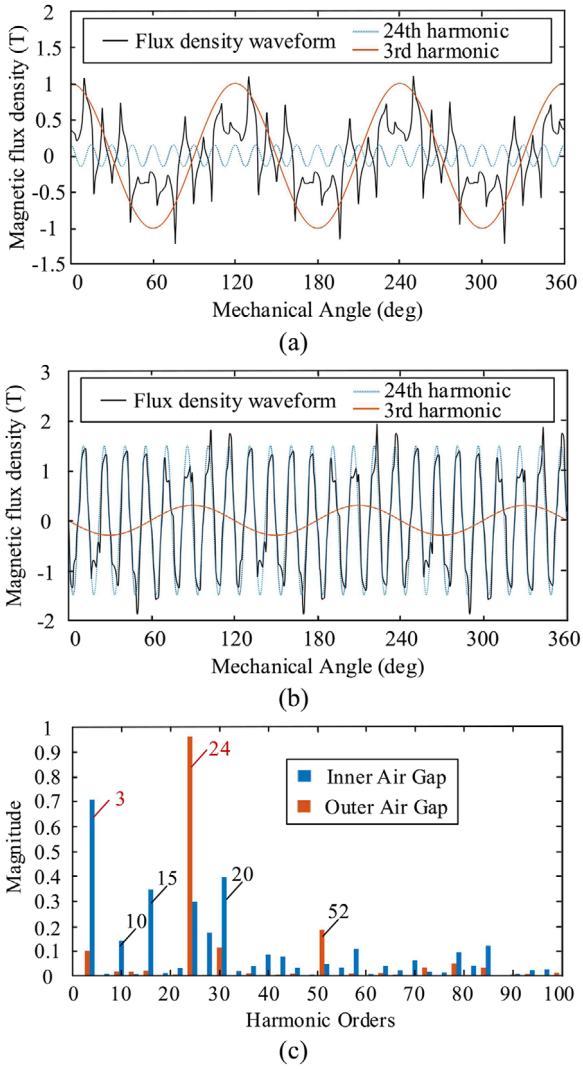

FIGURE 14 Radial air-gap flux density distribution. (a) Inner air gaps. (b) Outer air gaps. (c) Corresponding FFT analysis results

result shown in Figure 14c. Similarly, the magnetic flux density outer air gap also consists of third and 24th harmonics, while the domination harmonics become the 24th harmonic. Except for the main working harmonics as the red marks in Figure 14, the other harmonics are also shown.

4.2 | Torque performance

The relation between LSR and HSR torque of the proposed structure as well as the electrical angle is shown in Figure 15, showing a great torque-angle characteristic. The maximum output torque of HSR and LSR reaches 28.0 and 214.1 N·m, respectively. If the input torque or load torque is beyond these limits, the MG will lose its pace, and oscillation will occur.

Figure 16 shows the cogging torque of the two rotors, only reaching about 6.4% and 0.61% of the maximum torque generated by HSR and LSR.

17521424, 2022, 11, Downloaded from https://ietresearch.onlinelibrary.wiley.com/doi/10.1049/rpg2.12487 by Hong Kong Polytechnic University, Wiley Online Library on [27/08/2023]. See the Terms and Conditions (https://onlinelibrary.wiley.com/terms-and-conditions) on Wiley Online Library for rules of use; OA articles are governed by the applicable Creative Commons License

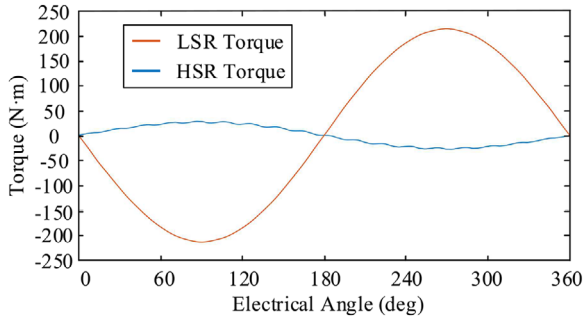

FIGURE 15 Relation between HSR and LSR torque as well as the electrical angle

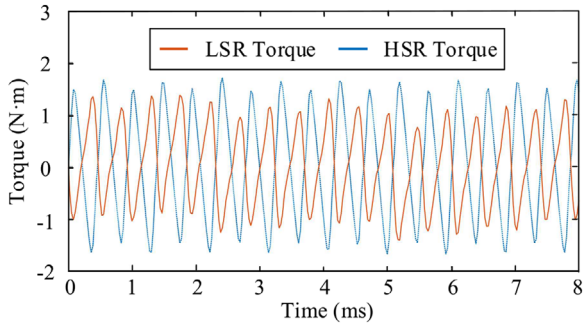

FIGURE 16 Cogging torque of two rotors

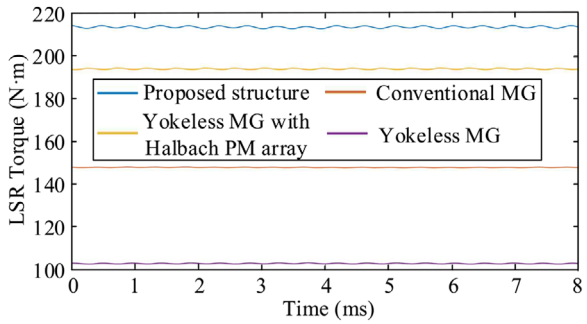

FIGURE 17 LSR torques comparison

The LSR and HSR torque of four MG are shown in Figures 17 and 18, including the conventional MG, yokeless MG, yokeless MG with Halbach PM as well as the proposed machine. The output torque of the proposed machine is the largest, followed by the yokeless MG with Halbach PM array, conventional MG, and yokeless MG.

Besides, the proposed structure also has a great ripple performance compared to yokeless MGs. A detailed parameter comparison under the working situation is shown in Table 4, where Motor I, II, III, and IV are conventional MG, yokeless MG, yokeless MG with Halbach PM array, and proposed machine. As shown in Table 4, the proposed structure has the best torque performance with torque and ripple, reaching 214 N·m and 0.7% (LSR) as well as 12.5% (HSR). Besides, the core loss of the proposed structure is reduced significantly compared to the conventional MG although it has the highest solid loss.

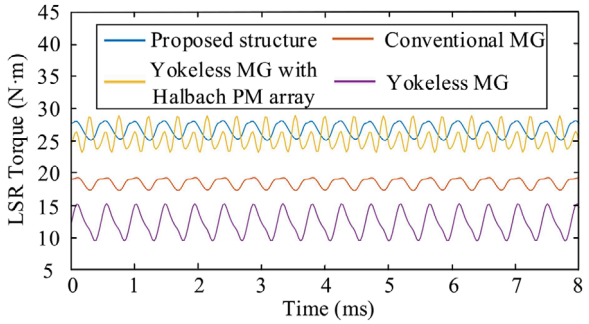

FIGURE 18 HSR torques comparison

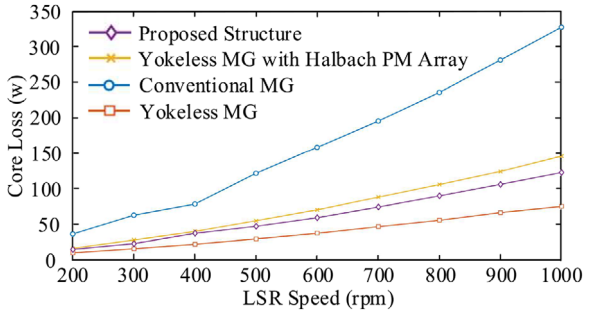

FIGURE 19 Core loss comparison

TABLE 4 Performance comparison results

	Model I	Model II	Model III	Model IV
Weight (kg)	3.36	2.72	3.13	3.26
Core loss (W)	63.72	15.3	27.6	22.5
Solid loss of PM (W)	42.9	55.2	146.3	157.3
Output torque (N·m)	147.2	102.3	193.8	214.1
LSR ripple	0.2%	0.8%	0.5%	0.7%
HSR ripple	11.1%	34.6%	21.2%	12.5%
PM weight (kg)	1.76	1.71	2.05	2.18
Iron weight (kg)	1.58	0.88	0.92	0.93
Supporter weight (kg)	0	0.152	0.154	0.149
Torque density (N·m/kg)	46.14	37.21	62.5	65.69
Torque density per PMs (N·m/kg)	96.31	57.48	96.13	95.65
Efficiency (%)	97.7	97.8	97.2	97.4

However, considering the solid loss and core loss, the proposed structure still has relatively high efficiency, reaching 97.4%. Furthermore, the proposed structure also has the highest torque density and the best anti-saturation capacity among those generalized MGs.

4.3 | Loss and efficiency comparison

Figure 19 shows the core loss of the proposed structure, yokeless MG with Halbach PM array, conventional MG, and

17521424, 2022, 11, Downloaded from https://ietresearch.onlinelibrary.wiley.com/doi/10.1049/rpg2.12487 by Hong Kong Polytechnic University, Wiley Online Library on [27/08/2023]. See the Terms and Conditions (https://onlinelibrary.wiley.com/terms-and-conditions) on Wiley Online Library for rules of use; OA articles are governed by the applicable Creative Commons License

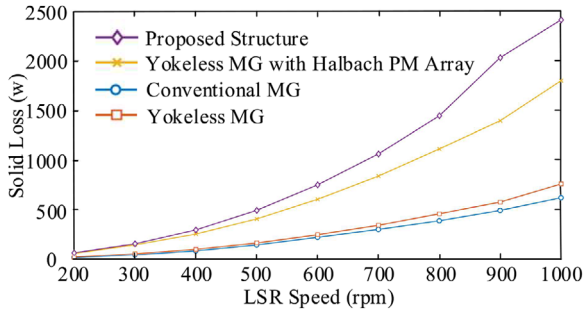

FIGURE 20 Solid loss comparison

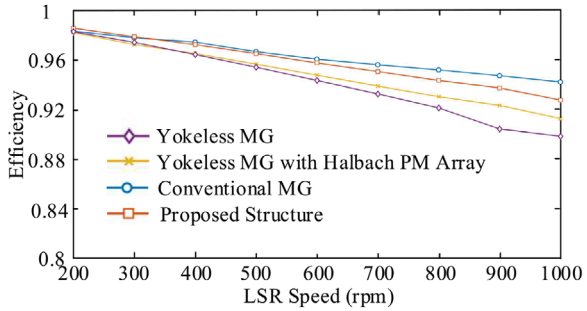

FIGURE 21 Efficiency comparison

yokeless MG with the LSR speed from 200 to 1000 rpm. Due to the yokeless structure, the core loss of yokeless MGs can be reduced sharply compared to conventional MG. Prominently, the proposed structure has the lowest core loss with the introduction of the embedded magnetic steel bar.

Figure 20 indicates the PM solid loss of those MGs versus LSR speed from 200 to 1000 rpm. All the solid loss of MGs will increase significantly with the increase in LSR speed. However, due to the asymmetric Halbach PM array, the proposed structure has the highest solid loss in particular with a higher LSR speed, followed by the yokeless MG with Halbach PM array, yokeless MG, and conventional MG.

Figure 21 shows the relations between the efficiency and LSR speed of those MGs, whose loss consists of the solid loss and the core loss.

As shown in Figure 21, the proposed structure has no advantage in terms of efficiency among four types of MGs and the gap between them is widen with the increase of LSR speed especially when the speed is larger than 500 rpm. Hence, the proposed structure is more applicable to be used in the direct-drive electric vehicle for its high torque density, high torque output capacity, and low torque ripple.

5 | CONCLUSION

This paper proposes a 3/27/24 yokeless MG with an asymmetric structure consisting of the trapezoidal Halbach PM array and embedded magnetic steel bar, which improves the performance significantly. First, the leakage flux of the proposed structure is reduced and the torque performance is improved with the introduction of the embedded magnetic steel bar by reducing the magnetic resistor of the magnetic circuit, reaching 214.1 N·m. Secondly, by using GFRP in place of silicon steel as the material of the rotor core, the torque density is improved significantly, reaching 59.28 N·m/Kg. Thirdly, the anti-saturation capacity of the MG with the proposed structure can be improved significantly compared to the yokeless MG with Halbach PM array. Finally, the iron loss and solid loss are carefully analyzed and compared. Considering the power efficiency, the proposed structure is more suitable to operate from the speed of 200 to 500 rpm, which indicates that it is more applicable to be used in low-speed high-torque applications.

ACKNOWLEDGEMENTS

This work was supported by the Research Grant Council of the Hong Kong SAR Government under projects PolyU PolyU152180/19E and PolyU152185/18E.

CONFLICT OF INTEREST

My coauthors and I do not have any conflict of interest to disclose.

DATA AVAILABILITY STATEMENT

The data that support the findings of this study are available from ANSYS. Restrictions apply to the availability of these data, which were used under license for this study. Data are available from the authors with the permission of ANSYS.

ORCID

Yuanxi Chen https://orcid.org/0000-0002-6531-9376

REFERENCES

1. Rotondale, A., Villani, M., Castellini, L.: Analysis of high-performance magnetic gears for electric vehicle. In: IEEE International Elec.Veh. Conference (IEVC), pp. 1–6 (2014)
2. Frandsen, T.V., et al.: Motor integrated permanent magnet gear in a battery electrical vehicle. IEEE Trans. Ind. App. 51(2), 1516–1525 (2015)
3. Guo, X., Liu, G.P., Shirazee, N., et al.: Electronic–magnetic gearing motor analyses and simulations for electric vehicle. IET Elec. Syst. Trans. 8(2), 95–100 (2018)
4. Chen, M., Chau, K., Liu, C.: Design and analysis of an advanced magnetic variable gear for hybrid electric vehicles. In: IEEE International Mag. Conference (INTERMAG), 1 (2015)
5. Jian, L., Xu, G., Wu, Y., Cheng, Z., Song, J.: A novel power-train using coaxial magnetic gear for power-split hybrid electric vehicles. In: International Conference on Electrical Machines and Systems, pp. 1–6 (2011)
6. Niu, S., Chen, N., Ho, S.L., Fu, W.N.: Design optimization of magnetic gears using mesh adjustable finite-element algorithm for improved torque. IEEE Trans. Magn. 48(11), 4156–4159 (2012)
7. Liu, Y., Ho, S.L., Fu, W.N.: A novel magnetic gear with intersecting axes. IEEE Trans. Magn. 50(11), 1–4, (2014)
8. Chen, Y., Fu, W.N., Ho, S.L., Liu, H.: A quantitative comparison analysis of radial-flux, transverse-flux, and axial-flux magnetic gears. IEEE Trans. Magn. 50(11), 1–4, (2014)
9. Chen, Y., Fu, W.N., Li, W.: Performance analysis of a novel triple-permanent-magnet- excited magnetic gear and its design method. IEEE Trans.Magn. 52(7), 1–4, (2016)
10. Liu, R., Zhao, Z., Sun, G., et al.: Exact magnetic field analytical model for eccentric magnetic harmonic gears using hyperbolic cotangent transformation. IET Electr. Power Appl. 14(4), 2667–2674 (2020)

17521424, 2022, 11, Downloaded from https://ietresearch.onlinelibrary.wiley.com/doi/10.1049/rpg2.12487 by Hong Kong Polytechnic University, Wiley Online Library on [27/08/2023]. See the Terms and Conditions (https://onlinelibrary.wiley.com/terms-and-conditions) on Wiley Online Library for rules of use; OA articles are governed by the applicable Creative Commons License

11. Mcgilton, B., Crozier, R., Mcdonald, A., et al.: Review of magnetic gear technologies and their applications in marine energy. IET Renew. Power Gener. 12(2), 174–181 (2018)
12. Liu, C., Chau, K.T., Lee, C.H.T., Song, Z.: A critical review of advanced electric machines and control strategies for electric vehicles. Proc. IEEE. 109(6), 1004–1028 (2021)
13. Zhu, Z.Q.: Overview of novel magnetically geared machines with partitioned stators. IET Electr. Power Appl. 12(5), 595–604 (2018)
14. Zhu, Z.Q., Khatab, M.F., Li, H., Liu, Y. A novel axial flux magnetically geared machine for power split application. IEEE Trans. Industry Appl. 54(6), 5954–5966 (2018)
15. Wang, Q., Niu, S., Yang, S.: Design optimization and comparative study of novel magnetic-geared permanent magnet machines. IEEE Trans.Magn. 53(6), 1–4 (2017)
16. Chen, Y., Fu, W.N., Li, W.: Performance analysis of a novel triple-permanent-magnet-excited magnetic gear and its design method. IEEE Trans. Magn. 52(7), 1–4 (2016)
17. Zhao, H., Liu, C., Dong, Z., Huang, R., Li, X.: Design and optimization of a magnetic-geared direct-drive machine with V-shaped permanent magnets for ship propulsion. IEEE Trans. Transport. Elec. 8(2), 1619–1633 (2021)
18. Jian, L., Chau, K.T., Gong, Yu, Jiang, J.Z., Yu, C., Li, W.: Comparison of coaxial magnetic gears with different topologies. IEEE Trans. Magn. 45(10), 4526–4529 (2009)
19. Fu, W.N., Li, L.: Optimal design of magnetic gears with a general pattern of permanent magnet arrangement. IEEE Trans. Appl. Supercond. 26(10), 1–6 (2016)
20. Ho, S.L., Niu, S., Fu, W.N.: Design and analysis of a novel axial-flux electric machine. IEEE Trans. Magn. 47(10), 4368–4371 (2011)
21. Zhao, X., Niu, S.: Design, optimization of a new magnetic-geared pole-changing hybrid excitation machine. IEEE Trans Ind. Electron. 64(12), 9943–9952 (2017)
22. Zhao, X., Niu, S., Fu, W.: Sensitivity analysis and design optimization of a new hybrid-excited dual-PM generator with relieving-DC-saturation structure for stand-alone wind power generation. IEEE Trans Magn. 56(1), 1–5 (2020)
23. Niu, S., Sheng, T., Zhao, X., Zhang, X.: Operation principle and torque component quantification of short-pitched flux-bidirectional-modulation machine. IEEE. Access. 7, 136676–136685 (2019)
24. Jing, L., Tang, W., Wang, T., Ben, T., Qu, R.: Performance analysis of magnetically geared permanent magnet brushless motor for hybrid electric vehicles. IEEE Trans. Transport. Elec. 8(2), 2874–2883 (2022)

How to cite this article: Chen, Y., Zhao, X., Ho, S., Niu, S., Fu, W.: Design and optimization of yokeless magnetic gear with asymmetric Halbach permanent magnet array for electric vehicle powertrain. IET Renew. Power Gener. 16, 2223–2232 (2022). https://doi.org/10.1049/rpg2.12487

17521424, 2022, 11, Downloaded from https://ietresearch.onlinelibrary.wiley.com/doi/10.1049/rpg2.12487 by Hong Kong Polytechnic University, Wiley Online Library on [27/08/2023]. See the Terms and Conditions (https://onlinelibrary.wiley.com/terms-and-conditions) on Wiley Online Library for rules of use; OA articles are governed by the applicable Creative Commons License